Biointerface Research in Applied Chemistry
Open-Access Journal (ISSN: 2069-5837)

Article
Volume 16, Issue 2, 2026, 67
https://doi.org/10.33263/BRIAC162.067

Diffusion-Thermo, and Chemical Reaction Effects on Transient Hydromagnetic Flow Past an Infinite Vertical Plate

Richa Deb Dowerah [1,*], Nazibuddin Ahmed [2], Masuma Khanam [3]

[1] Department of Mathematics, Gauhati University, Guwahati, 781014, Assam, India; debdowerahricha@gmail.com (R.D.D.); masuma.khanam09@gmail.com (M.K.);
[2] Department of Mathematics, Cotton University, Guwahati, 781001, Assam, India; nazib@gauhati.ac.in (N.A.);
* Correspondence: debdowerahricha@gmail.com;

Received: 31.10.2024; Accepted: 26.07.2025; Published: 15.04.2026

Abstract: A hydromagnetic, two-dimensional, unsteady flow having heat transfer and mass transfer characteristics of a viscous, incompressible, electrically conducting Boussinesq fluid flowing through an oscillating plate placed vertically and enclosed within a Darcian porous medium is considered, and analytical solutions are obtained. The fluid under consideration is a grey, non-scattering, radiating, emitting (or absorbing) medium. The chemical reaction, Dufour, and thermal radiation influences are also taken into account. The Laplace Transform Technique has been employed to find solutions subject to the dimensionless governing partial differential equations. The plate concentration and temperature are increased linearly with time(t) for t>0. The Dufour effect and thermal radiation are observed to have increased the thicknesses of the thermal and momentum boundary layers, but the heat transfer rate and shear stress are dominated by diffusion-thermo and thermal radiation effects, respectively. Also, it is noticeable that the chemical reaction parameter increases the Sherwood number, but dominates the concentration. The porosity parameter enhances fluid flow, and, as expected, the magnetic field decreases the fluid velocity. In the relativistic context, the motion of a high-speed vehicle, such as a missile or an airplane, may serve as an example of the flow problem we consider, where the infinite plate assumption is imposed. The current work also has a wide range of applications across many engineering fields, including civil engineering, mechanical engineering, and agricultural engineering.

Keywords: MHD; chemical reaction; heat and mass transfer; diffusion-thermo; porous media; radiation.

1. Introduction

Considering the numerous applications of magneto-hydrodynamics with mass and heat transfer, innumerable research studies have been carried out in this area. Kumar and Suneetha [1] numerically analyzed the influence of chemical reaction and thermal radiation on an MHD Williamson nanofluid over a stretching surface in the presence of a porous medium. Goud *et al*. [2] investigated mixed convective MHD flow of a fluid through an infinite vertical permeable plate along with the effects of chemical reaction, Joule heating, etc. Ilango and Lakshminarayana [3] examined the magnetic field effect on convective flow of a Casson fluid

over a stretching sheet with porous medium and viscous dissipation. The analysis of an unsteady MHD free convective flow across a semi-infinite permeable plate placed vertically in a Darcy–Forchheimer permeable medium is done by Sharma [4]. Unwanta *et al.* [5] studied the influence of variable thermal conductivity on a hydromagnetic fluid on a vertically placed, rotating cone, along with the effects of Soret, Dufour, and Darcy Forchheimer through a permeable medium. Seth *et al*. [6] conducted a study on an unsteady hydromagnetic free convection flow of an electrically conducting fluid past an exponentially accelerated vertical plate with ramped temperature through a permeable medium in the presence of thermal diffusion and Hall effects. Other noteworthy works on MHD include- Das *et al*. [7], Ali *et al*. [8,9], etc.

Diffusive processes, including the species' molecular diffusion in the presence of heterogeneous and homogeneous chemical reactions, are the means by which mass transfer occurs in many practical applications. A non-homogeneous reaction occurs in a small area or at the edge of a phase, whereas a homogeneous reaction occurs uniformly across a particular phase and is comparable to an internal heat source. For this reason, engineers and scientists in many other fields of science and engineering find it extremely useful to research heat and mass transfer along with chemical reactions. Mangamma *et al*. [10] aimed to study the effect of chemical reactions on fluid flow and heat transfer in an exponentially accelerated infinite plate subjected to vertical acceleration. Considering the effects of chemical reaction, viscous dissipation, Soret-Dufour, a study on MHD joule heating over an exponentially stretching sheet is contributed by Kumar *et al*. [11]. The influence of a first-order chemical reaction on a Newtonian fluid using the fractional Burgers' model is researched by Jiang *et al*. [12]. Sharma *et al*. [13] researched the n-th order chemical reaction on a steady hydromagnetic flow around a moving plate enclosed in a non-Darcian porous medium. Falodun and Ayegbusi [14] explored the flow of a chemically reacting nanofluid in a semi-infinite permeable plate, as well as the impacts of nonlinear buoyancy force and Soret-Dufour effects, which were checked using the spectral relaxation method. Saikia *et al*. [15] aimed at exploring thermal diffusion and chemical reaction on a free convective MHD flow that passes through an infinite permeable plate placed vertically within a porous medium. Kumar and Reddy [16] investigated the heat and mass transfer properties of a two-dimensional electrically conducting incompressible Maxwell fluid in the presence of chemical reaction, heat generation/absorption, and thermal radiation. Kumar *et al*. [17] conducted an outstanding study on non-Newtonian free convective MHD Casson fluid flow past a vertical porous plate in the existence of Soret, Dufour, and chemical reaction.

Many applications in geophysical and engineering fields involve flow through a permeable medium. For instance, flow through a permeable medium can be used in the department of engineering, like chemical sciences, to study purification and filtration processes; in petroleum technology, it can be used to observe the flow of water, oil, and natural gas through oil reservoirs; and in agricultural engineering, it can be utilized to study subterranean water resources. Numerous scholars have examined MHD free convective heat and mass transfer in porous media in light of these applications. Chamkha and Khaled [18] studied the problem of coupled heat and mass transfer by mixed convection in a linearly stratified stagnation flow (Hiemenz flow) of a fluid, with the plate surface embedded in a uniform Darcian porous medium. Das *et al*. [19] conducted an analytical study of the unsteady, convective MHD rotation of a non-Newtonian, electrically conducting Casson hybrid nanoliquid past a vertically placed porous plate. Mentioning other studies on porous media are

Vasu *et al*. [20], Huang [21], Jayaprakash *et al*. [22], Ahmed and Bordoloi [23], Seth *et al*. [24,25], Chamkha and Pop [26], Das *et al*. [27], Karmakar *et al.* [28] etc.

Diffusion-thermo is the term used to describe the energy flux that arises from concentration variations (Dufour effect). The Dufour effect is significant in many real-world applications, especially in the geosciences and chemical engineering, among other fields. Manthramurthy and Rao [29], Jiang *et al*. [30], Bejawada and Yanala [31], Appidi *et al*. [32], Bhattacharya *et al*. [33], Kumar *et al*. [34], Reddy and Kumar [35], and so on have contributed with their mind-blowing research in this area.

The present research article is an extension of the work done by Krishna *et al*. [36]. This investigation focuses on an unsteady hydromagnetic flow of a Newtonian, viscous, incompressible, electrically conducting fluid through an oscillating, infinite, vertical plate, embedded in a saturated, permeable medium, with varying mass diffusion and temperature. The effects of chemical reaction, Dufour, and thermal radiation are also checked. The novelty of the work is that we have taken the simultaneous effects of Dufour and chemical reaction into consideration. As far as our knowledge goes, several research papers have been published in the existing literature, but they have considered both effects independently. Furthermore, we have obtained an exact solution to the problem by adopting the Laplace Transform Technique. Such types of scenarios are very rare in the existing literature, hence proving the uniqueness of our work. Many fields of engineering, such as chemical, agricultural, civil, and mechanical engineering, as well as the oil and petroleum industry, would greatly benefit from the present investigation.

The present work may be reinvestigated by reducing the number of constraints and adopting modern numerical techniques such as the bvp4c method and the Crank-Nicolson method.

2. Materials and Methods

2.1. Mathematical formulation.

Figure 1 considers an unsteady hydromagnetic streamline boundary layer flow of a Newtonian, viscous, incompressible, electrically conducting fluid flowing through an oscillating, infinite, vertical plate enclosed within a saturated permeable medium, along with varying mass diffusion and temperature. The chemical reaction, Dufour, and thermal radiation effects are also observed. The x-axis has been considered vertically upward, i.e., parallel to the plate, and the z-axis orthogonal to the plate. The fluid and the plate are formerly supposed to be at identical concentration C_∞ temperature and temperature at all points being T_∞. After some time at t>0, an oscillatory motion with velocity $U_0 e^{i\omega t}$ is given to the plate in its own plane. Simultaneously, there is a linear increase in plate temperature with time t and a uniform mass diffusion from the plate. To idealize the model of this problem mathematically, we consider the following assumptions: a) It is assumed that a transverse magnetic field having uniform strength B_0 is implanted on the plate; b) The viscous dissipation and the induced magnetic field are insignificant considering the extremely low magnetic Reynolds number of the flow; c) The fluid under consideration is grey, absorbs and emits radiation, while not being a scattering medium.

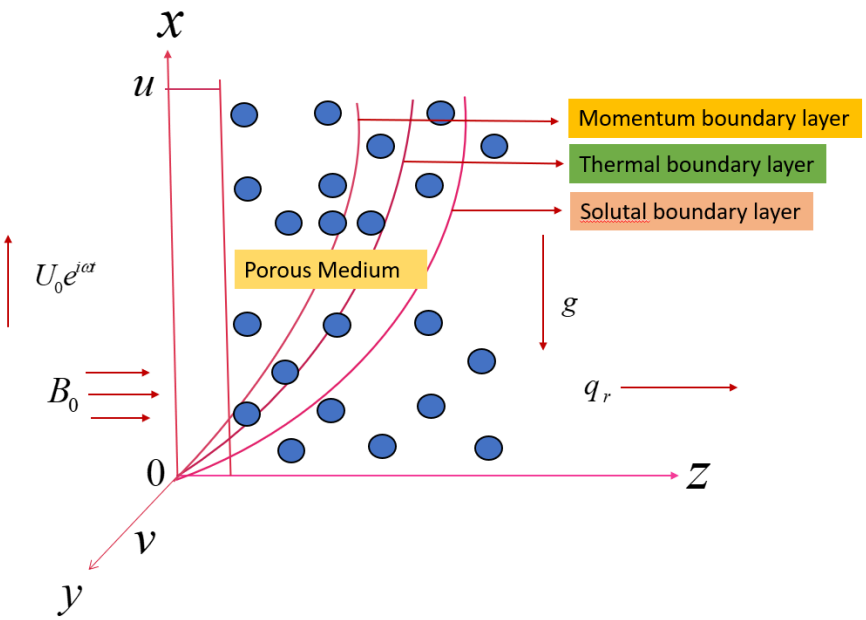

Figure 1. Physical configuration.

$$\frac{\partial u}{\partial t^*} = \nu \frac{\partial^2 u}{\partial z^{*2}} - (\frac{\sigma B_0^2}{\rho} + \frac{\nu}{k})u + g\beta(T - T_\infty) + g\beta_*(C - C_\infty) \quad (1)$$

$$\frac{\partial v}{\partial t^*} = \nu \frac{\partial^2 v}{\partial z^{*2}} - (\frac{\sigma B_0^2}{\rho} + \frac{\nu}{k})v \quad (2)$$

$$\rho C_p \frac{\partial T}{\partial t^*} = k_1 \frac{\partial^2 T}{\partial z^{*2}} - \frac{\partial q_r}{\partial z^*} + \frac{\rho D_M K_T}{C_S} \frac{\partial^2 C}{\partial z^{*2}} \quad (3)$$

$$\frac{\partial C}{\partial t^*} = D \frac{\partial^2 C}{\partial z^{*2}} + \overline{Kc}(C_\infty - C) \quad (4)$$

The local radiant absorption for optically thin, grey gas is as follows

$$\frac{\partial q_r}{\partial z^*} = -4a\sigma^*(T_\infty^4 - T^4) \quad (5)$$

Since it is supposed that temperature differences will be very small during the flow, so $T^4$is expanded about the free stream temperature (T_∞) using Taylor's series and ignoring the terms of high order as follows:

$$T^4 \cong 4T_\infty^3 T - 3T_\infty^4 \quad (6)$$

Using Eq. (5) and Eq. (6) in Eq. (3), the following equation is obtained:

$$\rho C_p \frac{\partial T}{\partial t^*} = k_1 \frac{\partial^2 T}{\partial z^{*2}} - 16a\sigma^* T_\infty^3 (T - T_\infty) + \frac{\rho D K_T}{C_S} \frac{\partial^2 C}{\partial z^{*2}} \quad (7)$$

The corresponding initial and boundary restrictions are expressed as follows:

$$\begin{gathered} u = 0, v = 0, T = T_\infty, C = C_\infty \; t \le 0 \forall z \\ u = U_0 e^{i\omega t}, v = 0, T = T_\infty + (T_w - T_\infty) \text{ at } C = C_\infty + (C_w - C_\infty) \text{ for } t > 0,\ z = 0 \\ u \to 0, v \to 0, T \to T_\infty, C \to C_\infty \text{ for } t > 0 \text{ as } z \to \infty \end{gathered} \quad (8)$$

Now, combining Eq. (1) and Eq. (2) and considering $q' = u + iv$, Eq. (9) is obtained:

$$\frac{\partial q'}{\partial t^*} = \nu \frac{\partial^2 q'}{\partial z^{*2}} - (\frac{\sigma B_0^2}{\rho} + \frac{\nu}{k})q' + g\beta(T - T_\infty) + g\beta^*(C - C_\infty) \quad (9)$$

The dimensionless quantities involved are as follows:

$$z = \frac{U_0 z^*}{\nu}, q = \frac{q'}{U_0}, \theta = \frac{T - T_\infty}{T_w - T_\infty}, \phi = \frac{C - C_\infty}{C_w - C_\infty}, Sc = \frac{\nu}{D}, Pr = \frac{\rho \nu C_p}{k_1},$$
$$M = \frac{\sigma B_0^2 \nu}{\rho U_0^2}, Gr = \frac{\nu g \beta (T_w - T_\infty)}{U_0^3}, Gm = \frac{\nu g \beta_* (C_w - C_\infty)}{U_0^3}, R = \frac{16 a \sigma^* \nu^2 T_\infty^3}{U_0^2 k_1},$$
$$K = \frac{U_0^2 k}{\nu^2}, t = \frac{U_0^2 t^*}{\nu}, Du = \frac{D K_T}{\nu C_s C_p (T_w - T_\infty)}, Kc = \frac{\nu \overline{Kc}}{U_0^2}.$$

Eq. (9), Eq. (7), and Eq. (4) are transformed to their respective dimensionless forms, i.e., Eq. (10), Eq. (11), and Eq. (12), with the help of the above dimensionless quantities:

$$\frac{\partial q}{\partial t} = \frac{\partial^2 q}{\partial z^2} - (M^2 + \frac{1}{K}) q + Gr\theta + Gm\phi \quad (10)$$
$$\frac{\partial \theta}{\partial t} = \frac{1}{Pr}\frac{\partial^2 \theta}{\partial z^2} - \frac{R}{Pr}\theta + Du\frac{\partial^2 \emptyset}{\partial z^2} \quad (11)$$
$$\frac{\partial \phi}{\partial t} = \frac{1}{Sc}\frac{\partial^2 \phi}{\partial z^2} - Kc\phi \quad (12)$$

The boundary restrictions stated in Eq. (8) are transformed through the dimensionless quantities as follows:

$$q = 0, \theta = 0, \phi = 0, t \leq 0 \forall z$$
$$q = e^{i\omega t}, \theta = 1, \phi = 1, \text{ for } t > 0, z = 0 \quad (13)$$
$$q \to 0, \theta \to 0, \ \phi \to 0, \text{ for } t > 0 \text{ as } z \to \infty$$

2.2. Solution procedure.

Applying the Laplace Transform to the non-dimensional governing equations in Eq. (10), (11), and (12), respectively, we get:

$$\frac{d^2 \bar{q}}{dz^2} - \left(M^2 + \frac{1}{K} + s\right)\bar{q} = -Gr\bar{\theta} - Gm\bar{\emptyset} \quad (14)$$

$$\frac{d^2 \bar{\theta}}{dz^2} - (R + sPr)\bar{\theta} = -DuSce^{-z\sqrt{Sc(s+Kc)}} - DuScKc\frac{e^{-z\sqrt{Sc(s+Kc)}}}{s} \quad (15)$$

$$\frac{d^2 \bar{\emptyset}}{dz^2} - (s + Kc)Sc\emptyset \quad (16)$$

Subject to the initial and boundary conditions:

$$\bar{q} = 0, \bar{\theta} = 0, \bar{\emptyset} = 0 \ \forall z,$$
$$\bar{q} = \frac{1}{s - i\omega}, \bar{\theta} = \frac{1}{s}, \bar{\emptyset} = \frac{1}{s} \text{ for } z = 0, \quad (17)$$
$$\bar{q} \to 0, \bar{\theta} \to 0, \ \bar{\emptyset} \to 0 \text{ as } z \to \infty.$$

On solving the equations. (14), (15), and (16) with the help of initial and boundary conditions, we get the following solutions:

$$\bar{q} = \left(\frac{1}{s - i\omega} - \frac{s_3}{(Pr - 1)(s + b)} - \frac{s_4}{(Sc - 1)(s + Kc)}\right)e^{-z\sqrt{M^2 + \frac{1}{K} + s}}$$
$$+ \frac{s_3}{(Pr - 1)(s + b)}e^{-z\sqrt{sPr + R}} + \frac{s_4}{(Sc - 1)(s + c)}e^{-z\sqrt{Sc(s+Kc)}} \quad (18)$$

$$\bar{\theta} = -\frac{s_3}{Gr}e^{-z\sqrt{Pr\left(s+\frac{R}{Pr}\right)}} - DuScs_1e^{-z\sqrt{Sc(s+Kc)}} - DuScKcs_2e^{-z\sqrt{Sc(s+Kc)}} \quad (19)$$

$$\bar{\emptyset} = \frac{1}{s}e^{-z\sqrt{Sc(s+Kc)}} \quad (20)$$

Where:

$$s_1 = \frac{1}{s(Sc-Pr)+ScKc-R}, s_2 = \frac{s_1}{s}, s_3 = -Gr(\frac{1}{s} + DuScs_1 + DuScKcs_2),$$

$$s_4 = Gr(DuScs_1 + DuScKcs_2) - \frac{Gm}{s}$$

Next, apply the inverse Laplace transformation to the equations. (18), (19), and (20) respectively, we get the following solutions for velocity, temperature, and concentration:

$$q = q_1 + q_2 + q_3 \quad (21)$$

$$\theta = L_1 + L_2 + L_3 - L_4 - L_5 \quad (22)$$

$$\emptyset = \psi_1 \quad (23)$$

Where:

$$L_1 = \psi_2, L_2 = \frac{DuSc}{Sc-Pr}\psi_3, L_3 = \frac{DuScKc}{Sc-Pr}(A_1\psi_2 + A_2\psi_3)$$

$$L_4 = \frac{DuSc}{Sc-Pr}\psi_4, L_5 = \frac{DuScKc}{Sc-Pr}(A_1\psi_1 + A_2\psi_4)$$

$$q_1 = q_{11} + q_{12} + q_{13}$$

And:

$$q_{11} = \psi_5, \; q_{12} = \frac{Gr}{Pr-1}(q_{121} + q_{122} + q_{123})$$

Here:

$$q_{121} = A_{10}\psi_6 + A_{11}\psi_{11}, \; q_{122} = \frac{DuSc}{Sc-Pr}(A_{12}\psi_7 + A_{13}\psi_{11}),$$

$$q_{123} = \frac{DuScKc}{Sc-Pr}(A_{14}\psi_6 + A_{15}\psi_7 + A_{16}\psi_{11}), \; q_{13} = \frac{1}{1-Sc}(q_{131} + q_{132} + q_{133})$$

And:

$$q_{131} = \frac{GrDuSc}{Sc-Pr}(A_3\psi_7 + A_4\psi_8), \; q_{132} = \frac{GrDuScKc}{Sc-Pr}(A_5\psi_6 + A_6\psi_7 + A_7\psi_8),$$

$$q_{133} = -Gm(A_8\psi_6 + A_9\psi_8),$$

Next:

$$q_2 = \frac{Gr}{1-Pr}(q_{21} + q_{22} + q_{23}),$$

Where:

$$q_{21} = A_{10}\psi_2 + A_{11}\psi_9, q_{22} = \frac{DuSc}{Sc-Pr}(A_{12}\psi_3 + A_{13}\psi_9),$$

$$q_{23} = \frac{DuScKc}{Sc-Pr}(A_{14}\psi_2 + A_{15}\psi_3 + A_{16}\psi_9)$$

Again:

$$q_3 = \frac{1}{Sc-1}(q_{31} + q_{32}),$$

$$q_{31} = \frac{GrDuSc}{Sc-Pr}(q_{311} + q_{312}), \; q_{311} = A_3\psi_4 + A_4\psi_{10},$$

$$q_{312} = Kc(A_5\psi_1 + A_6\psi_4 + A_7\psi_{10}), \; q_{32} = -Gm(A_8\psi_1 + A_9\psi_{10})$$

We have:

$$\psi(Sc, Kc, z, t) = \frac{1}{2}[e^{\sqrt{ScKc}z}erfc(\frac{\sqrt{Sc}z}{2\sqrt{t}} + \sqrt{Kct}) + e^{-\sqrt{ScKc}z}erfc(\frac{\sqrt{Sc}z}{2\sqrt{t}} - \sqrt{Kct})],$$

$$\psi(Pr,\frac{R}{Pr},z,t)=\frac{1}{2}[e^{\sqrt{R}z}erfc(\frac{\sqrt{Pr}z}{2\sqrt{t}}+\sqrt{\frac{R}{Pr}t})+e^{-\sqrt{R}z}erfc(\frac{\sqrt{Pr}z}{2\sqrt{t}}-\sqrt{\frac{R}{Pr}t})],$$

$$e^{-at}\,\psi(Pr,\frac{R}{Pr}-a,z,t)=\frac{1}{2}e^{-at}[e^{\sqrt{\Pr\left(\frac{R}{Pr}-a\right)}z}erfc(\frac{\sqrt{Pr}z}{2\sqrt{t}}+\sqrt{\left(\frac{R}{Pr}-a\right)t})+$$
$$e^{-\sqrt{\Pr\left(\frac{R}{Pr}-a\right)}z}erfc(\frac{\sqrt{Pr}z}{2\sqrt{t}}-\sqrt{\left(\frac{R}{Pr}-a\right)t}$$

$$e^{-at}\psi(Sc,Kc-a,z,t)$$
$$=\frac{1}{2}e^{-at}[e^{\sqrt{Sc(Kc-a)}z}erfc\left(\frac{\sqrt{Sc}z}{2\sqrt{t}}+\sqrt{(Kc-a)t}\right)$$
$$+e^{-\sqrt{Sc(Kc-a)}z}erfc(\frac{\sqrt{Sc}z}{2\sqrt{t}}-\sqrt{(Kc-a)t})]$$

$$e^{i\omega t}\psi(1,M^2+\frac{1}{K}+i\omega,z,t)=\frac{1}{2}e^{i\omega t}[e^{\sqrt{\left(M^2+\frac{1}{K}+i\omega\right)}z}erfc(\frac{z}{2\sqrt{t}}+\sqrt{\left(M^2+\frac{1}{K}+i\omega\right)t})$$
$$+e^{-\sqrt{(M^2+\frac{1}{K}+i\omega)}z}erfc(\frac{z}{2\sqrt{t}}-\sqrt{(M^2+\frac{1}{K}+i\omega)t})]$$

$$\psi(1,M^2+\frac{1}{K},z,t)=\frac{1}{2}[e^{\sqrt{\left(M^2+\frac{1}{K}\right)}z}erfc(\frac{z}{2\sqrt{t}}+\sqrt{\left(M^2+\frac{1}{K}\right)t})$$
$$+e^{-\sqrt{(M^2+\frac{1}{K})}z}erfc(\frac{z}{2\sqrt{t}}-\sqrt{(M^2+\frac{1}{K})t})]$$

$$e^{-at}\psi(1,M^2+\frac{1}{K}-a,z,t)=\frac{1}{2}e^{-at}[e^{\sqrt{(M^2+\frac{1}{K}-a)}z}erfc(\frac{z}{2\sqrt{t}}+\sqrt{(M^2+\frac{1}{K}-a)t})+$$
$$e^{-\sqrt{(M^2+\frac{1}{K}-a)}z}\,erfc(\frac{z}{2\sqrt{t}}-\sqrt{(M^2+\frac{1}{K}-a)t})]$$

$$e^{-ct}\psi(1,M^2+\frac{1}{K}-c,z,t)=\frac{1}{2}e^{-ct}[e^{\sqrt{\left(M^2+\frac{1}{K}-c\right)}z}erfc(\frac{z}{2\sqrt{t}}+\sqrt{\left(M^2+\frac{1}{K}-c\right)t})$$
$$+e^{-\sqrt{(M^2+\frac{1}{K}-c)}z}erfc(\frac{z}{2\sqrt{t}}-\sqrt{(M^2+\frac{1}{K}-c)t})]$$

$$e^{-bt}\,\psi(Pr,\frac{R}{Pr}-b,z,t)=\frac{1}{2}e^{-bt}[e^{\sqrt{\Pr\left(\frac{R}{Pr}-b\right)}z}erfc(\frac{\sqrt{Pr}z}{2\sqrt{t}}+\sqrt{\left(\frac{R}{Pr}-b\right)t})+$$
$$e^{-\sqrt{\Pr\left(\frac{R}{Pr}-b\right)}z}erfc(\frac{\sqrt{Pr}z}{2\sqrt{t}}-\sqrt{\left(\frac{R}{Pr}-b\right)t}$$

$$e^{-ct}\psi(Sc,Kc-c,z,t)=\frac{1}{2}e^{-ct}[e^{\sqrt{Sc(Kc-c)}z}erfc(\frac{\sqrt{Sc}z}{2\sqrt{t}}+\sqrt{(Kc-c)t})$$
$$+e^{-\sqrt{Sc(Kc-c)}z}erfc(\frac{\sqrt{Sc}z}{2\sqrt{t}}-\sqrt{(Kc-c)t})]$$

$$e^{-bt}\psi(1,M^2+\frac{1}{K}-b,z,t)=\frac{1}{2}e^{-bt}[e^{\sqrt{\left(M^2+\frac{1}{K}-b\right)}z}erfc(\frac{z}{2\sqrt{t}}+\sqrt{\left(M^2+\frac{1}{K}-b\right)t})$$

$$+e^{-\sqrt{(M^2+\frac{1}{K}-b)z}}erfc(\frac{z}{2\sqrt{t}}-\sqrt{(M^2+\frac{1}{K}-b)t})],$$

$$R=\frac{4+3N}{3N}, a=\frac{ScKc-R}{Sc-Pr}, b=\frac{R-M^2-\frac{1}{K}}{Pr-1}, c=\frac{ScKc-M^2-\frac{1}{K}}{Sc-1}, A_1=\frac{1}{a}, A_2=-A_1, A_3=\frac{1}{c-a},$$
$$A_4=-A_3, A_5=\frac{1}{ac}, A_6=\frac{1}{a(a-c)}, A_7=\frac{1}{c(c-a)}, A_8=\frac{1}{c}, A_9=-A_8, A_{10}=\frac{1}{b},$$
$$A_{11}=-A_{10}, A_{12}=\frac{1}{b-a}, A_{13}=-A_{12}, A_{14}=\frac{1}{ab}, A_{15}=\frac{1}{a(a-b)}, A_{16}=\frac{1}{b(b-a)}.$$

2.3. Skin friction.

Skin friction, also known as drag force, is given by:

$$\tau=-\frac{\partial q}{\partial z}\Big|_{z=0} \quad (24)$$

2.4. Nusselt number.

With the aid of the conduction law given by Fourier, the Nusselt number (heat transfer rate) is:

$$Nu=-\frac{\partial \theta}{\partial z}\Big|_{z=0} \quad (25)$$

2.5. Sherwood number.

Also referred to as mass transfer rate, the Sherwood number is:

$$Sh=-\frac{\partial \phi}{\partial z}\Big|_{z=0} \quad (26)$$

3. Results and Discussions

In an attempt to gain a thorough grasp of the problem, several numerical computations for the species concentration, energy, and momentum equations, the Nusselt number, skin friction, and the Sherwood number have been carried out, along with the assignment of specific values to the variables. The Prandtl number's values are taken to be 0.7 (for air), 3 (for some liquid), and 4.34 (for water), where the Prandtl number (Pr) is a dimensionless quantity representing the ratio of momentum diffusivity to thermal diffusivity in a fluid. It represents the significance of momentum and heat transfer in fluid flow and plays a pivotal role in understanding boundary layer behavior. Likewise, we have considered the values 0.22, 0.6, and 0.78 for Schmidt number, and it is crucial to remember that 0.22 is the Schmidt number value for hydrogen (H_2), 0.6 for water vapor (H_2O), and 0.78 for ammonia (NH_3). Now, like the Prandtl number, the Schmidt number (Sc) is also a dimensionless quantity representing the ratio of momentum diffusivity (kinematic viscosity) to mass diffusivity. A higher Schmidt number indicates that momentum diffuses more easily than mass, but a lower Schmidt number depicts the opposite. All figures and tables in this section present the computed results.

3.1. Velocity analysis.

Keeping the other parameters constant, as we increase the magnetic parameter values in Figures 2 and 3, the fluid velocity starts to fall. Now, the reason for this behavior is a force called the Lorentz force, a resistive force produced when an electrically conducting fluid is

subjected to a magnetic field applied transversely. The force in question tends to decelerate the fluid's velocity in the boundary layer.

Also, another observation can be made from Figure 2 that although the fluid velocity declines with the increment of magnetic strength. Still, this decrement becomes slow in every step i.e., as we increase the value of 'M' from 2 to 3 it can be seen that the velocity curve falls drastically than in case of the increment of 'M' from 3 to 4. The same observation is evident in Figure 3 as well, but it is more pronounced in Figure 2.

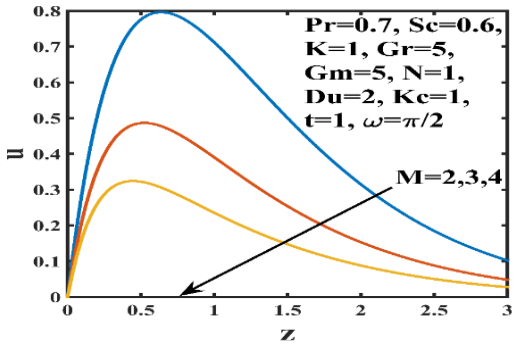

Figure 2. Velocity layout vs. height for different magnetic parameters M (u vs z).

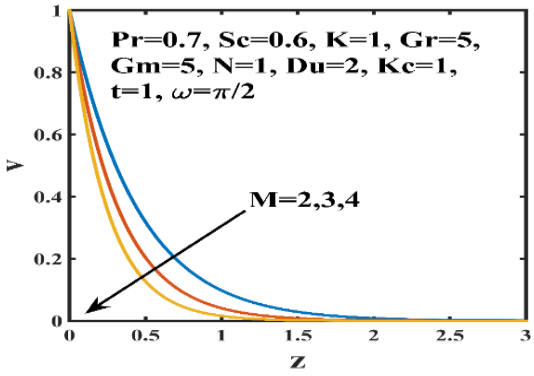

Figure 3. Velocity layout vs. height for different magnetic parameters M (v vs z).

A complete reversal of behavior from Figures 2 and 3 is evident in Figure 4. Fluid velocity increases with increasing permeability; i.e., the more permeable a medium is, the faster the fluid flows through it.

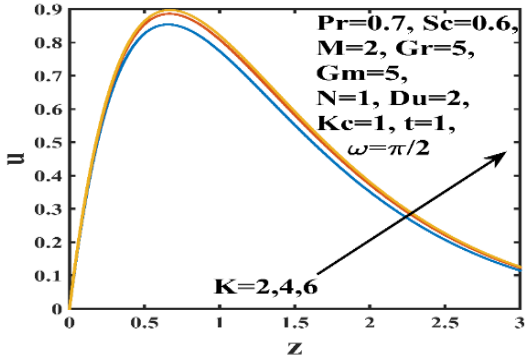

Figure 4. Velocity layout vs. height for different porosity parameters K (u vs z).

Figure 5 displays the velocity response to various values of thermal Grashof number, Gr. The results show that an upsurge in the value of 'Gr' increases the fluid velocity. 'Gr' is a dimensionless quantity that indicates the buoyancy-to-viscous force ratio applied to a fluid in the boundary layer. The boundary layer becomes laminar with greater values of 'Gr'. The increasing thermal buoyancy force has caused the velocity profile to rise upward, as predicted.

Furthermore, when ‘Gr’ increases, the fluid's velocity increases fast in the surroundings of the porous plate before gradually decreasing to the free stream velocity.

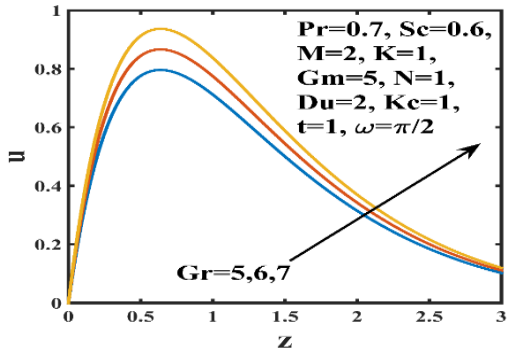

Figure 5. Velocity layout vs. height for different thermal Grashof number values, Gr (u vs z).

Figure 6 shows the typical boundary-layer velocity patterns for a range of solutal Grashof numbers, Gm, clearly indicating an increase in velocity with increasing solutal boundary-layer thickness. The velocity distribution clearly peaks closer to the plate surface. It then appropriately declines to get nearer to the value of the free stream.

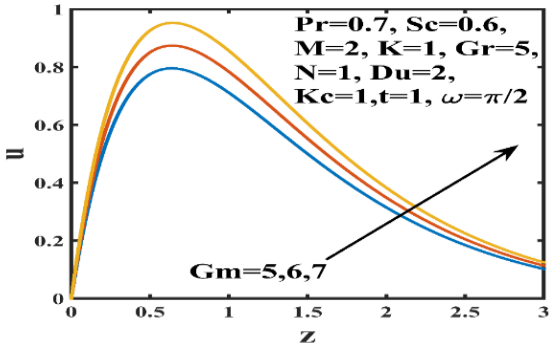

Figure 6. Velocity layout vs. height for different solutal Grashof number Gm values (u vs z).

The increment of the Dufour effect leads to acceleration of the fluid’s velocity, as shown in Figure 7. This happens because, as the Dufour number rises, the convection current strengthens, increasing the fluid velocity.

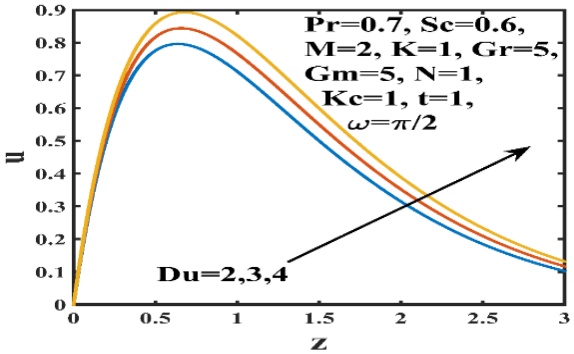

Figure 7. Velocity layout vs. height for different Dufour parameters Du (u vs z).

The demonstration of Figure 8 leads to the conclusion that the thermal radiation effect increases the fluid’s velocity. Another observation is that the fluid velocity increases more rapidly when N increases from 1 to 2 than from 2 to 3; i.e., there comes a point at which the increase in fluid velocity becomes almost negligible, even as we keep increasing N.

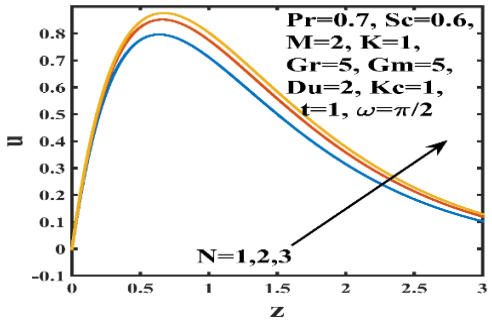

Figure 8. Velocity layout vs. height for different thermal Radiation parameters N (u vs z).

The frequency parameter $'\omega'$ dominates the fluid velocity in Figure 9. Also, it can be noticed that as we move ahead through the horizontal axis, the increment or decrement of velocity with respect to $''\omega'$ becomes negligible.

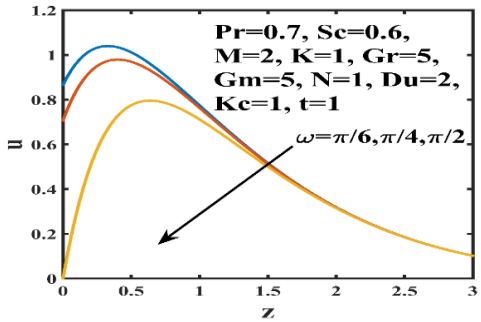

Figure 9. Velocity layout for various values of ω (u vs z).

Unlike Figure 9, velocity is dominated by the frequency parameter 'ω' in Figure 10, i.e., the effect of 'ω' shows contrasting behaviors for the real and imaginary parts of velocity (Figure 9 and Figure 10).

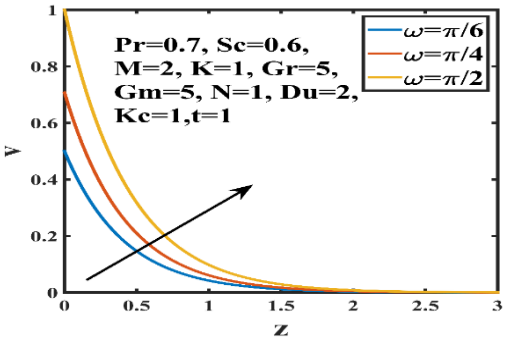

Figure 10. Velocity layout for different values of ω (v vs z).

3.2. Temperature effects.

The temperature rises with increasing diffusion-thermo, thermal radiation, and time, as seen in Figures 11, 12, and 13, respectively. An interesting fact about these graphs is that the more we keep increasing the values of thermal radiation and time, the smaller the increase in temperature.

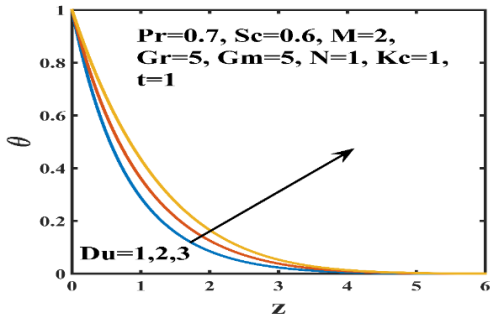

Figure 11. Temperature layout for different Dufour parameter values Du.

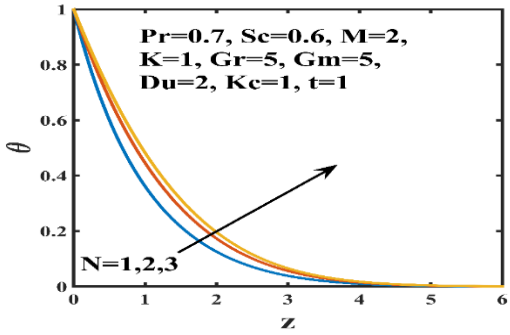

Figure 12. Temperature layout for different thermal radiation values N.

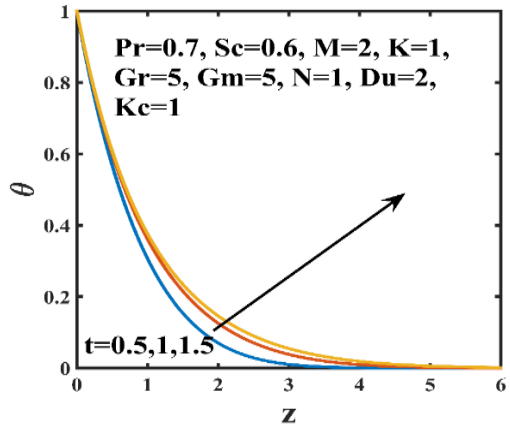

Figure 13. Temperature layout for different times t.

Figure 14 demonstrates that the thermal boundary profile decreases with increasing momentum diffusivity.

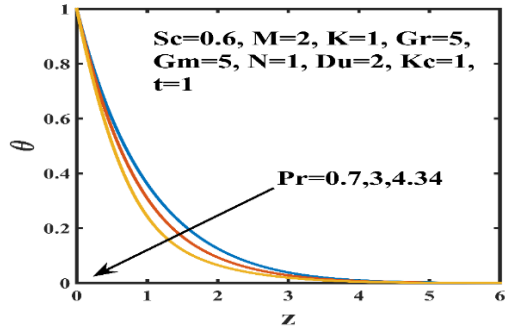

Figure 14. Temperature layout for different Prandtl number values, Pr.

3.3. Concentration analysis.

Figures 15 and 16 show the Schmidt number and chemical reaction effects on the solutal boundary. High 'Sc' values will physically correlate with a fluid's decreasing molecular

diffusivity, which will slow the pace at which species diffuse. Since lower 'Sc' values are associated with higher molecule diffusivities, they will have the opposite effect. As a result, as 'Sc' hikes, the concentration boundary layer thickness significantly drops. Additionally, the concentration buoyancy effects diminish as the chemical reaction parameter 'Kc' rises, causing a decline in fluid concentration (Figure 16).

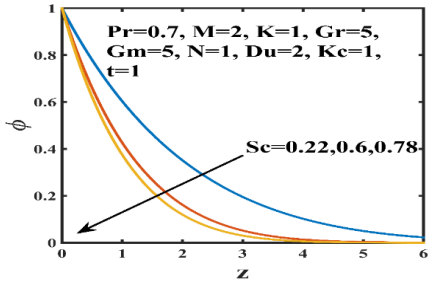

Figure 15. Concentration layout for several Schmidt number values, Sc.

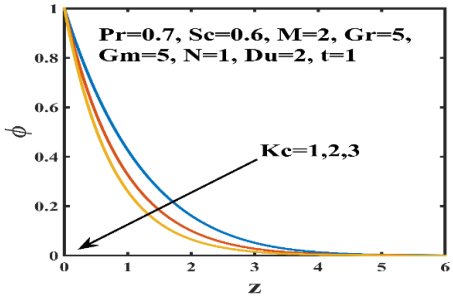

Figure 16. Concentration layout for various chemical reaction parameter values Kc.

3.4. Sherwood number influences.

The Sherwood number graph for various values of Schmidt number in Figure 17 shows that 'Sh' is highest for NH_3, then for H_2O, and finally it is the lowest for H_2, i.e., with the upsurge of 'Sc', 'Sh' also increases.

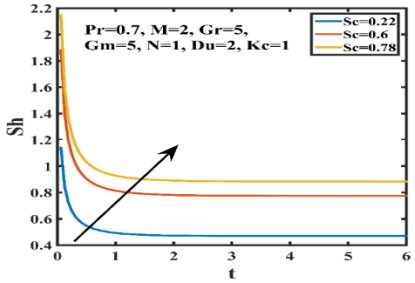

Figure 17. Sherwood number layout for several Schmidt number values, Sc.

With the increase in chemical reaction parameters, the Sherwood number also increases (as shown in Figure 18), assuming the other parameters are constant.

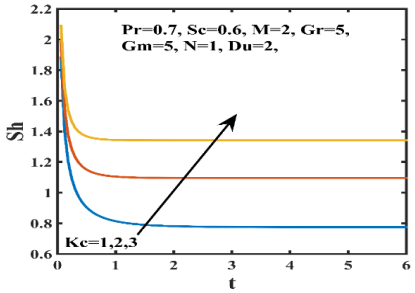

Figure 18. Sherwood number profile for various chemical reaction parameter values Kc.

3.5. Nusselt number analysis.

We have considered two tables (Table 1 and Table 2) for observing the influence of several parameters on the Nusselt number. Table 1 is for Sc=0.22, which indicates that both the Dufour parameter and the radiation parameter decline the heat transfer rate, but the upsurge of 'Pr' leads to improvement of the Nusselt number.

Table 1. Numerical values of Nusselt number(Nu) with Sc=0.22, Gr=5, M=2, Gm=5, Kc=1, t=1.

Du	Pr	N	Nu
1	0.70	1	1.45
2	0.70	1	1.37
3	0.70	1	1.29
2	**0.70**	1	1.37
2	**3.00**	1	1.43
2	**4.34**	1	1.54
2	0.70	**1**	1.37
2	0.70	**2**	1.08
2	0.70	**3**	0.97

On the other hand, Table 2 is for Sc=0.6, and in this table only the effect of 'Du' has been studied since it shows contradicting behaviors for hydrogen and water vapor, i.e., for Sc=0.6 the diffusion-thermo effect enhances the heat transfer rate, unlike for Sc=0.22.

Table 2. Numerical values of Nusselt number(Nu) for Pr=0.7, Gr=5, M=2, Sc=0.6, Gm=5, Du=2, N=1, Kc=1, t=1.

Du	Nu
1	2.10
2	2.66
3	3.23

3.6. Skin friction coefficient analysis.

To study the influence of several variables, the skin friction coefficient values corresponding to these parameters are listed in Table 3. It can be easily declared from the table that all the parameters, viz., the magnetic parameter, diffusion-thermo, and rotational parameter, decrease the skin friction coefficient at the plate, except for the thermal Grashof number.

Table 3. Skin friction coefficient, τ (numerical values) for Pr=0.7, K=1, Sc=0.6, Gm=2, N=1, Kc=1, t=1.

M	Gr	Du	ω	τ
2	2	1	π/2	-0.02
3	2	1	π/2	-0.43
4	2	1	π/2	-0.44
2	**2**	1	π/2	-0.02
2	**3**	1	π/2	0.23
2	**4**	1	π/2	0.47
2	2	**1**	π/2	-0.02
2	2	**2**	π/2	-0.93
2	2	**3**	π/2	-1.88
2	2	1	**π/6**	2.20
2	2	1	**π/4**	1.79
2	2	1	**π/2**	-0.02

3.7. Comparison Graph.

In order to validate our findings, we have compared our figure (Figure 19) to Figure 10 of Bordoloi *et al*. [37] by keeping the values of magnetic parameter M=2,6,10,14,18 in our figure (Figure 19) as well, i.e., same as Figure 10 of Bordoloi *et al*. [37]. Now, ignoring the other parameters, it can be distinctly observed that for an increasing value of magnetic

parameter 'M', fluid velocity declines in both cases. This means that our figure is in good agreement with that of Bordoloi *et al*. [37], which is enough to prove the validation of our work.

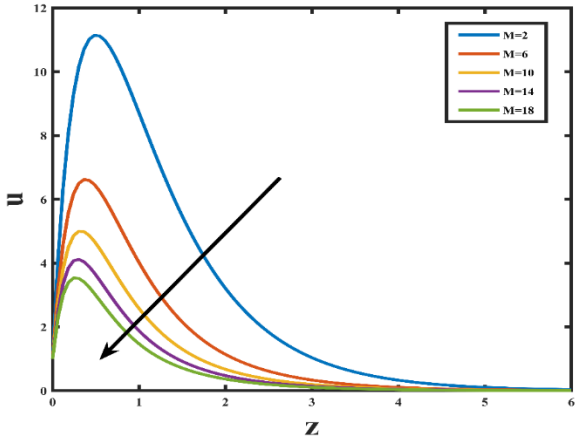

Figure 19. Comparison figure for fluid velocity for different values of magnetic Parameter M (Author's Figure)

3.8. Comparison Table.

3.8.1. Comparison of the results of Velocity.

For various values of thermal Grashof number, Gm, the change in the values of velocity (third column of Table 4) has been tabulated in Table 4 by considering the Dufour parameter, Du and chemical reaction parameter, Kc to be zero and then it has been compared to the results of the base paper, Krishna *et al*. [36] (second column of Table 4). It can be clearly observed from the table that the velocity values in both papers increase with increasing thermal Grashof number, Gm. Also, these values of velocity are almost the same for a given value of the thermal Grashof number, Gm. Therefore, it can be concluded that our results for the velocity are in good agreement with those of the base paper for varying values of the thermal Grashof number, Gm.

Table 4. Comparison for the results of velocity for M=0.5, K=0.5, Sc=0.22, R=1, t=1, z=2, ωt=π/2, Gm=5, Pr=0.71, Du=0, Kc=0.

Gm	Base Paper results Krishna *et al.* [36]	Present paper results
5	0.384775	0.384780
7	0.432589	0.432591
10	0.547087	0.547143

3.8.2. Comparison of the results of temperature.

Assuming the values of other parameters to be some non-zero constants, Dufour parmater, Du and chemical reaction parameter, Kc to be zero and for rising values of Prandtl number, Pr, the values of temperature (third column of Table 5) has been tabulated in Table 5 and then it has been compared to the values of temperature of the base paper (second column of temperature) for the same values of non dimensional parameters as the present paper.

Table 5. Comparison of the results of temperature for t=1, z=2, R=0.5, Du=0, Kc=0.

Pr	Base Paper results Krishna *et al.* [36]	Present paper results
0.71	0.0711681	0.0711793
3	0.0025271	0.0025282
7	0.0000186	0.0000190

From both papers, it can be seen that the temperature decreases with increasing Prandtl number, Pr, and that the values of temperature for a particular Prandtl number, Pr, are almost

the same. Hence, it can be concluded that our results for temperature match those of the base paper.

3.8.3. Comparison of the results of Concentration.

Again, considering the other parameters to be some non-zero constants, the Dufour parameter, Du and the chemical reaction parameter, Kc to be zero, the values of concentration (third column of Table 6) has been tabulated in Table 6 for increasing values of Schmidt number, Sc and then it has been compared to the values of concentration of the base paper (second column of Table 6) for the same values of non dimensional parameters as the present paper. It can be clearly seen from the table that the concentration values in both papers decrease with increasing Schmidt number, Sc, and for the same Schmidt number, Sc, the concentration values are almost the same. Therefore, considering all the above mentioned factors in the current paragraph, it can be concluded that our results matches with that of the results of the base paper.

Table 6. t=1, z=2, Du=0, Kc=0.

Sc	Base Paper results Krishna *et al.* [36]	Present the paper results
0.22	0.284447	0.284443
0.6	0.164551	0.164565
0.78	0.081447	0.081478

4. Conclusions

The present study considers the influences of chemical reactions and diffusion-thermo on a transient hydromagnetic flow over a vertical, oscillating plate. Some of the noteworthy findings of this investigation are that the magnetic field effect diminishes the fluid velocity along the x-direction by 75% as we increase the value of the magnetic parameter, 'M', from 2 to 4, while the buoyancy forces enhance it by approximately 30% as we increase the value of the Grashof number from 5 to 7. The diffusion-thermo effect enhances both the thermal and the momentum boundary layer thicknesses. The frequency parameter decelerates the fluid velocity. The thermal radiation effect increases both velocity and temperature. The thermal boundary layer is decreased by the Prandtl number. The solutal boundary layer decelerates with the increment of chemical reaction.

Future research can be carried out on our work by implementing the effects of both Dufour and Soret simultaneously with the inclusion of viscous dissipation and Ohmic dissipation, which should be solved numerically as problems with simultaneous implementation of Soret and Dufour effects results in the coupling of Energy equation and Species' Continuity equation hence leading to a infeasible solution when solved with the help of Laplace Transform Technique.

Author Contributions

Conceptualization, R.D.D. and N.A.; methodology, R.D.D. and N.A.; software, R.D.D.; validation, N.A.; formal analysis, R.D.D.; investigation, R.D.D.; resources, R.D.D.; data curation, N.A., R.D.D., and M.K.; writing—original draft preparation, R.D.D.; writing—review and editing, N.A., R.D.D., and M.K.; visualization, R.D.D., N.A., and M.K.; supervision, N.A.; project administration, N.A. All authors have read and agreed to the published version of the manuscript.

Institutional Review Board Statement

Not applicable.

Informed Consent Statement

Not applicable.

Data Availability Statement

No new data were created or analyzed in this study. Data sharing is not applicable.

Funding

This research received no external funding.

Acknowledgments

The authors heartfully acknowledge Dr. Rajdeep Bordoloi for his valuable advice while preparing the manuscript. Also, the consent of Dr. Rajdeep Bordoloi has been taken for mentioning his name in this section.

Conflicts of Interest

The authors declare no conflict of interest.

Abbreviations

The following abbreviations are used in this manuscript:

Abbreviation	Definition
C	Concentration (kg m^{-3})
C_p	Specific Heat at Constant Pressure ($Jkg^{-1}K$)
C_∞	Free Stream Concentration (kg m^{-3})
C_w	Concentration at the Wall (kg m^{-3})
a	Spectral Mean Absorption Coefficient of the Medium
σ*	Stefan-Boltzman Constant
G_r	Thermal Grashof Number
Du	Dufour Parameter
K_T	Thermal Diffusion Ratio
R	Radiation Conduction Parameter
C_S	Concentration Susceptibility
k_1	Thermal Conductivity ($Wm^{-1}K^{-1}$)
K	Porosity Parameter
M	Magnetic Parameter
Pr	Prandtl Number
D	Mass Diffusivity (m^2s^{-1})
q_r	Radiative Heat Flux
R	Radiation Parameter
G_m	Solutal Grashof Number
S_c	Schmidt Number
k	Permeability of the Porous Medium
T	Fluid Temperature (K)
t	Non-Dimensional Time
Kc	Chemical Reaction Parameter
T_∞	Free Stream Temperature (K)
g	Acceleration due to Gravity (ms^{-2})

Abbreviation	Definition
N	Thermal Radiation Parameter
u	Dimensionless Velocity Along X-Axis (ms^{-1})
T_w	Wall Temperature
v	Dimensionless Velocity Along Y-Axis
β	Volumetric Co-Efficient for Thermal Expansion (K^{-1})
β_*	Volumetric Co-Efficient for Solutal Expansion (K^{-1})
ν	Kinematic Viscosity (m^2s^{-1})
ω	Frequency Parameter
ρ	Density (kgm^{-3})
θ	Dimensionless Fluid Temperature
σ	Electrical Conductivity 1/mΩ)
ϕ	Dimensionless Fluid Concentration

Subscripts

The following subscripts are used in this manuscript:

Subscripts	Definition
∞	Condition at Infinity
w	Conditions on the Wall

References

1. Kumar, B.P.; Suneetha, S. Numerical Investigation of Diffusion Thermo and Thermal Diffusion on MHD Convective Flow of Williamson Nanofluid on a Stretching Surface through a Porous Medium in the Presence Chemical Reaction and Thermal Radiation. *J. Adv. Res. Fluid Mech. Thermal Sci.* **2024**, *115*, 141-157, https://doi.org/10.37934/arfmts.115.2.141157.
2. Goud, B.S.; Reddy, Y.D.; Asogwa, K.K. Inspection of chemical reaction and viscous dissipation on MHD convection flow over an infinite vertical plate entrenched in porous medium with Soret effect. *Biomass Conv. Bioref.* **2024**, *14*, 7683-7694, https://doi.org/10.1007/s13399-022-02886-3.
3. Ilango, M.S.; Lakshminarayana, P. Induced magnetic field and Soret–Dufour effects on viscous dissipative Casson fluid flow through porous medium over a stretching sheet. *J. Therm. Anal. Calorim.* **2024**, *149*, 8713-8727, https://doi.org/10.1007/s10973-024-13352-9.
4. Sharma, R. Transient MHD Free Convection Flow, Heat and Mass Transfer in Darcy–Forchheimer Porous Medium in the Presence of Chemical Reaction and Heat Absorption with Soret and Dufour Effects: Element-Free Galerkin Modelling. *Math. Model. Comput. Simul.* **2023**, *15*, 357-372, https://doi.org/10.1134/S2070048223020151.
5. Uwanta, I.J.; Yale, I.D.; Ahmed, A. Effects of Variable Thermal Conductivity on MHD Fluid Flow on Rotating Vertical Cone in the Presence of Darcy Forchheimer, Soret and Dufour Effects through a Porous Medium. *Phys. Sci. Int. J.* **2024**, *28*, 1-20, https://doi.org/10.9734/psij/2024/v28i4832.
6. Seth, G.S.; Tripathi, R.; Sharma, R. Natural Convection Flow Past an Exponentially Accelerated Vertical Ramped Temperature Plate with Hall Effects and Heat Absorption. *Int. J. Heat Tehnol.* **2015**, *33*, 139-144, http://doi.org/10.18280/ijht.330321.
7. Das, S.; Ali, A.; Jana, R.N. Impact of hall currents with buoyancy forces on hydromagnetic reactive casson fluid flow past a slippery plate in a rotating porous medium. *Spec. Top. Rev. Porous Media Int. J.* **2020**, *11*, 313-340, https://doi.org/10.1615/SpecialTopicsRevPorousMedia.2020029405.
8. Ali, A.; Jana, R.N.; Das, S. Hall effects on radiated magneto-power-law fluid flow over a stretching surface with power-law velocity slip effect. *Multidiscip. Model. Mater. Struct.* **2020**, *17*, 103-125, https://doi.org/10.1108/MMMS-01-2020-0005.
9. Ali, A.; Banerjee, S.M.; Das, S. Hall and ion slip current's impact on magneto-sodium alginate hybrid nanoliquid past a moving vertical plate with ramped heating, velocity slip and Darcy effects. *Multidiscip. Model. Mater. Struct.* **2020**, *17*, 65-101, https://doi.org/10.1108/MMMS-12-2019-0218.
10. Mangamma, C.; Pramod Kumar, P.; Malga, B.S.; Appidi, L.; Matta, S. Effect of Dufour and chemical reaction on an unsteady magneto hydrodynamics flow past an exponentially moving plate. *Heat Transfer* **2024**, *53*, 1689-1708, https://doi.org/10.1002/htj.23010.

11. Kumar, D.; Sinha, S.; Sharma, A.; Agrawal, P.; Kumar Dadheech, P. Numerical study of chemical reaction and heat transfer of MHD slip flow with Joule heating and Soret–Dufour effect over an exponentially stretching sheet. *Heat Transfer* **2022**, *51*, 1939-1963, https://doi.org/10.1002/htj.22382.
12. Jiang, Y.; Sun, H.G.; Bai, Y.; Zhang, Y. MHD flow, radiation heat and mass transfer of fractional Burgers' fluid in porous medium with chemical reaction. *Comput. Math. Appl.* **2022**, *115*, 68-79, https://doi.org/10.1016/j.camwa.2022.01.014.
13. Sharma, B.R.; Choudhury, R.; Das, U.J. Soret–Dufour effects on chemically reacting non-Darcian MHD flow around a plate. *Heat Transfer* **2023**, *52*, 28-39, https://doi.org/10.1002/htj.22684.
14. Falodun, B.O.; Ayegbusi, F.D. Soret–Dufour mechanism on an electrically conducting nanofluid flow past a semi-infinite porous plate with buoyancy force and chemical reaction influence. *Numer. Methods Partial Differential Eq.* **2021**, *37*, 1419-1438, https://doi.org/10.1002/num.22588.
15. Saikia, D.J.; Ahmed, N.; Bordoloi, R. Natural convective mhd mass transfer flow past an infinite vertical porous plate embedded in a porous medium with thermal diffusion and chemical reaction. *Spec. Top. Rev. Porous Media Int. J.* **2023**, *14*, 63-75, https://doi.org/10.1615/SpecialTopicsRevPorousMedia.2023045885.
16. Kumar, M.A.; Reddy, Y.D. Thermal radiation and chemical reaction influence on MHD boundary layer flow of a Maxwell fluid over a stretching sheet containing nanoparticles. *J. Therm. Anal. Calorim.* **2023**, *148*, 6301-6309, https://doi.org/10.1007/s10973-023-12097-1.
17. Kumar, M.A.; Reddy, Y.D.; Goud, B.S.; Rao, V.S. An impact on non-Newtonian free convective MHD Casson fluid flow past a vertical porous plate in the existence of Soret, Dufour, and chemical reaction. *Int. J. Ambient Energy* **2022**, *43*, 7410-7418, https://doi.org/10.1080/01430750.2022.2063381.
18. Chamkha, A.J.; Khaled, A.-R.A. Similarity solutions for hydromagnetic mixed convection heat and mass transfer for Hiemenz flow through porous media. *Int. J. Numer. Methods Heat Fluid Flow* **2000**, *10*, 94-115, https://doi.org/10.1108/09615530010306939.
19. Das, S.; Ali, A.; Jana, R.N. Insight into the dynamics of magneto-casson hybrid nanoliquid caused by a plate rotation. *World J. Eng.* **2021**, *18*, 66-84, https://doi.org/10.1108/WJE-07-2020-0261.
20. Vasu, B.; Gorla, R.S.R; Murthy, P.V.S.N.; Prasad, V.R.; Bég, O.A.; Siddiqa, S. MHD Free Convection-Radiation Interaction in a Porous Medium - Part II: Soret/Dufour Effects. *Int. J. Appl. Mech. Eng.* **2020**, *25*, 157-175, https://doi.org/10.2478/ijame-2020-0027.
21. Huang, J.S. Chemical reaction and activation energy on heat and mass transfer for convective flow along an inclined surface in Darcy porous medium with Soret and Dufour effects. *J. Mech.* **2023**, *39*, 88-104, https://doi.org/10.1093/jom/ufad006.
22. Jayaprakash, J.; Govindan, V.; Santra, S.S.; Askar, S.S.; Foul, A.; Nandi, S.; Hussain, S.M. Thermal radiation, Soret and Dufour effects on MHD mixed convective Maxwell hybrid nanofluid flow under porous medium: a numerical study. *Int. J. Numer. Methods Heat Fluid Flow* **2024**, *34*, 3924-3952, https://doi.org/10.1108/HFF-03-2024-0229.
23. Ahmed, N.; Bordoloi, R. Three-dimensional flow past a porous vertical plate in a porous medium with sinusoidal suction and permeability in the presence of thermal diffusion. *Heat Transfer* **2022**, *51*, 677-700, https://doi.org/10.1002/htj.22325.
24. Seth, G.S.; Kumbhakar, B.; Sarkar, S. Unsteady MHD natural convection flow with exponentially accelerated free-stream past a vertical plate in the presence of hall current and rotation. *Rend. Circ. Mat. Palermo, II. Ser* **2017**, *66*, 263-283, https://doi.org/10.1007/s12215-016-0250-1.
25. Seth, G.S.; Sarkar, S.; Sharma, R. Effects of Hall current on unsteady hydromagnetic free convection flow past an impulsively moving vertical plate with Newtonian heating. *Int. J. Appl. Mech. Eng.* **2016**, *21*, 187-203, https://doi.org/10.1515/ijame-2016-0012.
26. Chamkha, A.J.; Pop, I. Effect of thermophoresis particle deposition in free convection boundary layer from a vertical flat plate embedded in a porous medium. *Int. Commun. Heat Mass Transf.* **2004**, *31*, 421-430, https://doi.org/10.1016/j.icheatmasstransfer.2004.02.012.
27. Das, S.; Ali, A.; Jana, R.N. Darcian slip flow of rotating magnetoreactive PEG conveying MoS_2 casson nanofluid with ramped temperature and concentration. *Spec. Top. Rev. Porous Media Int. J.* **2020**, *11*, 71-102, https://doi.org/10.1615/SpecialTopicsRevPorousMedia.2020030547.
28. Karmakar, P.; Das, S.; Mahato, N.; Ali, A.; Jana, R.N. Dynamics prediction using an artificial neural network for a weakly conductive ionized fluid streamed over a vibrating electromagnetic plate. *Eur. Phys. J. Plus* **2024**, *139*, 407, https://doi.org/10.1140/epjp/s13360-024-05197-w.

29. Manthramurthy, P.; Rao, S. Thermophoresis & Soret-DuFour on MHD Mixed Convection of a Nano Fluid with a Porous Medium over a Stretching Sheet with a Non-Uniform Heat Source/Sink. *Int. J. Appl. Math. Theor. Phys.* **2024**, *10*, 1-20, https://doi.org/10.11648/j.ijamtp.20241001.11.
30. Jiang, Y.; Sun, H.; Zhang, Y. Convection heat and mass transfer of non-Newtonian fluids in porous media with Soret and Dufour effects using a two-sided space fractional derivative model. *Comput. Math. Appl.* **2024**, *173*, 74-86, https://doi.org/10.1016/j.camwa.2024.08.004.
31. Bejawada, S.G.; Yanala, D.R. Finite element Soret Dufour effects on an unsteady MHD heat and mass transfer flow past an accelerated inclined vertical plate. *Heat Transfer* **2021**, *50*, 8553-8578, https://doi.org/10.1002/htj.22290.
32. Appidi, L.; Malga, B.S.; Matta, S.; Kumar, P.P. Heat and mass transfer for Soret and Dufour's consequences on unsteady MHD free convection flow over a porous media with heat absorption. *Heat Transfer* **2021**, *50*, 8492-8505, https://doi.org/10.1002/htj.22286.
33. Bhattacharyya, A.; Kumar, R.; Seth, G.S. Capturing the features of peristaltic transport of a chemically reacting couple stress fluid through an inclined asymmetric channel with Dufour and Soret effects in presence of inclined magnetic field. *Indian J. Phys.* **2021**, *95*, 2741-2758, https://doi.org/10.1007/s12648-020-01936-8.
34. Kumar, M.A.; Reddy, Y.D.; Goud, B.S.; Rao, V.S. Effects of soret, dufour, hall current and rotation on MHD natural convective heat and mass transfer flow past an accelerated vertical plate through a porous medium. *Int. J. Thermofluids* **2021**, *9*, 100061, https://doi.org/10.1016/j.ijft.2020.100061.
35. Reddy, M.S.; Kumar, M.A. Influence of magnetic field chemical reaction and Soret-Dufour parameters on Maxwell nanofluid flow over a porous vertical stretching surface-A numerical study. *Case Stud. Chem. Environ. Eng.* **2024**, *10*, 100958, https://doi.org/10.1016/j.cscee.2024.100958.
36. Krishna, M.V.; Reddy, M.G.; Chamkha, A.J. HEAT AND MASS TRANSFER ON UNSTEADY MHD FLOW THROUGH AN INFINITE OSCILLATING VERTICAL POROUS SURFACE. *J. Porous Media* **2021**, *24*, 81-100, https://doi.org/10.1615/JPorMedia.2020025021.
37. Bordoloi, R.; Chamuah, K.; Ahmed, N. Free Convective MHD Radiative Flow Past a Porous Vertical Plate in a Porous Medium with Chemical Reaction. *Biointerface Res. Appl. Chem.* **2023**, *13*, 259, https://doi.org/10.33263/BRIAC133.259.

Publisher's Note & Disclaimer